Scripta Materialia 243 (2024) 115970

Contents lists available at ScienceDirect

Scripta Materialia

journal homepage: www.journals.elsevier.com/scripta-materialia

Asymmetrical magnetization processes induced by compositional gradients in ferromagnetic nanowires

Claudia Fernández-González [a,b,1], Alba Berja [c,1], Laura Álvaro-Gómez [a,d,f], Carolina Martín-Rubio [e], Arantzazu Mascaraque [f], Lucía Aballe [g], Ruy Sanz [e], Lucas Pérez [a,f,*], Sandra Ruiz-Gómez [b,**]

[a] Instituto Madrileño de Estudios Avanzados - IMDEA Nanociencia, C/ Faraday 9, Madrid, 28049, Spain
[b] Max Planck Institute for Chemical Physics of Solids, Nöthnitzer Str. 40, Dresden, 01187, Germany
[c] Instituto de Ceramica y Vidrio (CSIC), C/ Kelsen 5, Madrid, 28049, Spain
[d] Univ. Grenoble Alpes, CNRS, CEA, Grenoble INP, SPINTEC, Grenoble, 38000, France
[e] Instituto Nacional de Técnica Aeroespacial - INTA, Torrejón de Ardoz, Madrid, 28850, Spain
[f] Dpto. Física de Materiales, Universidad Complutense de Madrid, Plaza de las Ciencias 1, Madrid, 28040, Spain
[g] Alba Synchrotron Light Facility, CELLS, Carrer de la Llum 2-26, Cerdanyola del Vallès, 08290, Barcelona, Spain

ARTICLE INFO

Keywords:
Electrodeposition
Nanowires
Ratchet effect
Magnetization processes

ABSTRACT

Electrodeposited nanowires are an excellent scenario to study and control magnetic domain wall motion in nanostructures. In particular, the introduction of local changes in composition during the growth procedure has been proven to be very efficient for controlling the magnetization dynamics. In this work, we show the possibility of introducing compositional gradients in FeNi electrodeposited nanowires by gradually changing the Fe/Ni ratio along their axis. These compositional gradients produce an asymmetrical landscape for domain wall motion which is reflected in asymmetrical magnetization processes under an applied magnetic field. By studying nanowires with different compositional gradients we were able to correlate composition and magnetic asymmetry. Our results pave the way towards full control of the movement of domain walls along the nanowires.

The control of magnetization processes is key in developing novel magnetic devices. In particular, full control of the movement of domain walls (DWs) along elongated nanostructures under magnetic field or spin-polarized currents is on the basis of a novel generation of spintronics devices. Up to now, most of the studies on magnetization dynamics in these systems have been focused on 2-dimensional elongated structures with square cross-section — nanostripes — looking for applications in logic [1,2] or magnetic storage devices [3,4]. In order to manipulate the dynamics of domain walls within these systems, local changes in the geometry of the nanostripes are introduced. These geometrical notches are strategically placed along the axis of the nanostripes to create targeted changes in the local energy of the domain walls, thus acting as local pinning sites [5]. To fully harness domain wall motion, it is crucial to take a further step in the design process. This involves developing devices where information travels only in a single, predetermined direction [6]. This *domain wall ratchet effect* has been reported in different 2-dimensional magnetic structures by introducing asymmetric energy landscapes for domain wall motion: triangular submicrometric antidots in thin films [7], changes in shape anisotropy induced by piezoelectric materials in heterostructures [8] or introducing local changes of anisotropy in nanostrips [9].

In recent years, 3D magnetic systems [10] and curvilinear nanostructures [11] have appeared as exciting alternatives for developing novel spintronics applications. Nanowires (NWs) are among the most studied curvilinear systems. In these systems, it is possible to stabilize complex topologically protected domain walls [12], giving rise to novel effects like the suppression of the speed limit for the domain wall movement, the so-called *Walker Breakdown* [13]. Magnetic NWs can be easily fabricated by template-assisted electrodeposition [14,15], a technique that allows control of the geometry and composition of the NWs, and thus tailoring their magnetization configuration [16–19].

* Corresponding author at: Dpto. Física de Materiales, Universidad Complutense de Madrid, Plaza de las Ciencias 1, Madrid, 28040, Spain.
** Corresponding author.
E-mail addresses: lucas.perez@ucm.es (L. Pérez), Sandra.Gomez@cpfs.mpg.de (S. Ruiz-Gómez).
[1] These two authors contributed equally to this work.

https://doi.org/10.1016/j.scriptamat.2024.115970
Received 7 July 2023; Received in revised form 6 December 2023; Accepted 4 January 2024
Available online 16 January 2024

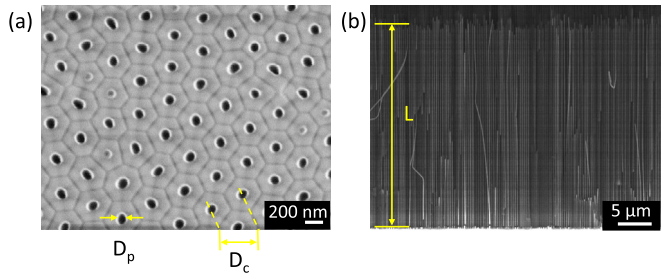

Fig. 1. SEM micrograph of: (a) top view of the alumina templates used for electrodeposition. Pore diameter ($D_p = 100 \pm 10$ nm) and interpore distance ($D_C = 300 \pm 10$ nm) are shown. (b) Cross section of the system after the electrodeposition process. The length of the nanowires ($L = 30$ μm) is shown.

Regarding the control of domain wall motion, two strategies have been mainly used: the introduction of geometrical [20,21] or compositional changes along the axis of the nanowires [22–24]. In both cases, the local energy of domain walls along the axis is modified, creating efficient local pinning sites for domain wall motion. Also it is possible to introduce asymmetric energy landscapes for *a ratchet effect* in the domain wall motion by introducing asymmetrical changes in the diameter along the axis [19,25].

This *ratchet effect* has been previously reported in ferromagnetic FeCo/Cu NWs in which an asymmetry is introduced along the axial direction by increasing the lengths of magnetostatically coupled ferromagnetic segments [26]. In this system, the ratchet effect is produced by the different reversal fields of the segments due to the asymmetrical landscape of the magnetostatic coupling. However, for real applications, it would be very beneficial to have all segments with the same length — same bit length. In addition, it would also be interesting to have an asymmetric landscape for domain wall energy, producing the ratchet effect by controlling the domain wall motion instead of the remagnetization of the ferromagnetic segments. In this work, we demonstrate asymmetrical magnetization processes in ferromagnetic Fe-Ni NWs by introducing compositional gradients along the axial direction, i.e., gradually changing the Fe/Ni ratio of the alloy along the axis. The design and magnetic characteristics of these NWs make them suitable for real device applications.

Arrays of FeNi NWs were electrodeposited using Anodized Aluminium Oxide (AAO) as nanoporous templates. AAO templates were prepared by hard anodization, from 500 μm-thick Al disks, with a purity of 99.999% (Goodfellow). After cleaning and electropolishing, the disks were anodized in a 0.3 M oxalic acid and ethanol solution at $0-1\,^{\circ}C$, with an applied potential of 140 V for 150 min. Afterwards, the remaining Al was removed by chemical etching in a 1:4 mixture of $CuCl_2$ and HClO and the pores opened with H_3PO_4 5% vol. at 35 °C for 75 min. Following this procedure, the final diameter of the pores of the AAO templates is around 100 nm. A top view of an example of a template used is shown in Fig. 1.a.

Electrodeposition was carried out at room temperature in a three-electrode electrochemical cell, using a Pt mesh as a counter electrode and a Ag/AgCl (3 M NaCl) electrode as a reference electrode. Before electrodeposition, a Ti(10 nm)/Au(200 nm) film was sputtered on one side of the membrane to act as working electrode. The Au layer was thickened up to 1 μm using electrodeposition to increase the conductivity of the electrode. The electrolyte used is composed of $NiSO_4$ (0.8 M) and $NiCl_2$ (0.02 M) as Ni^{2+} sources, $FeSO_4$ (0.02 M) as Fe^{2+} source and H_3BO_3 (0.4 M) as additive. All chemicals were of analytical grade and mixed in deionized water without further purification. The pH was adjusted to 2.3 using H_2SO_4 10% vol. The electrodeposited NWs have a diameter of 100 nm, and they follow the hexagonal order of the template, with a distance between each other of 300 nm, measured from center to center (see Fig. 1.a). A cross section of the template after the growth of the nanowires is shown in Fig. 1.b.

The morphology of the NWs was studied by Scanning Electron Microscopy (SEM) using a Carl Zeiss SIGMA y 6335F JEOL microscope. The composition was quantified by Scanning Transmission Electron Microscopy (STEM) using a JEOL JEM 3000F microscope. Transmission X-ray microscopy (TXM) was performed at the MISTRAL beamline of the ALBA Synchrotron, equipped with a transmission X-ray microscope operating in the soft X-ray range that utilizes photons extracted from a bending magnet source [27]. The NWs were deposited flat on top of a X-ray-transparent silicon nitride membrane mounted in a sample holder installed at the microscope. For these studies, the NWs were released from the templates, removing first the Au contact layer by wet etching with a I_2 (0.1M) and KI (0.6M) water-based solution and afterwards the template, also by wet etching, using a H_3PO_4 (0.4M) and H_2CrO_4 (0.2M) solution.

The composition of electrodeposited Fe-Ni NWs can be controlled during growth by changing the applied potential [28]. However, considering the anomalous codeposition and its dependence on geometry, it is essential to establish the relationship between the composition of the Fe-Ni alloy and the potential for each particular geometry. For that, we have grown Fe-Ni NWs using the already described AAO templates and two different electrolytes, with different relative Fe^{2+} concentrations (16% and 28% related to the total number of electroactive ions (Fe^{2+} y Ni^{2+}) in the electrolyte), varying the growth potential from −0.9 V to −1.5 V. The composition of the samples, measured by Energy-dispersive X-ray spectroscopy, is plotted in Fig. 2.a as a function of the growth potential, together with the relative concentration of Fe in the electrolyte for both electrolytes (horizontal lines). The composition has been measured in large areas, with large concentration of nanowires, after releasing the NWs from the templates. Therefore, it should be considered as an average of the composition of each array of NWs. As expected, there is clear evidence for anomalous codeposition in all samples, as the relative Fe concentration in the samples is much higher than the relative concentration of Fe^{2+} in the electrolyte [29]. As reported in previous works [28], at low overpotentials, there is a large Fe concentration in the alloy whereas, when increasing the potential and electrodeposition moves towards the mass-transport-controlled region, curves approach a constant Fe concentration, whose value is close to the Fe:Ni ratio of the electrolyte. From the figure, it is clear that significant changes in composition, and thus in the saturation magnetization, are expected when changing the growth potential from −0.9 V to −1.5 V, making possible the introduction of a compositional gradient in the nanowire and so, a gradient in the saturation magnetization.

The growth rate also depends on the growth potential. Therefore, before growing the samples with compositional gradients we calibrate the growth rate by measuring the length of nanowires deposited with different growth potentials for the electrolyte containing a 16% of Fe^{2+}. Fig. 2.b collects the measured deposition rate as a function of the potential. As expected, the evolution of the growth rate follows the behavior of the cathodic electrochemical current predicted by the Butler-Volmer equation. Considering this dependence of growth rate on potencial, pulse plating (using pulses of variable voltage and length) should be used for creating and controlling compositional gradients. Fig. 2.c shows an example of two of these pulse trains.

A sketch of a segment grown under the application of one of these pulses is shown in Fig. 2.d. The color-code corresponds to the color-code shown in Fig. 2.c for the different potential pulses. The vertical axis shows an approximate atomic percentage of Ni (green) and Fe (red) along the nanowire axis. Specifically, it can be observed that low overpotentials correspond to Fe-rich regions. The composition gradually shifts from a Fe-rich one towards a Ni-rich alloy. Once the variation of composition has been established, the length of the pulses can be varied by applying a factor, producing larger or smaller compositional gradients. In particular, three different samples have been grown in this work. In all cases, the Fe content varies from 65% to 10% in segments of 1 μm, 2 μm, and 4 μm, respectively. The number of segments was repeated in all cases for a final nanowire's length of 30 μm.

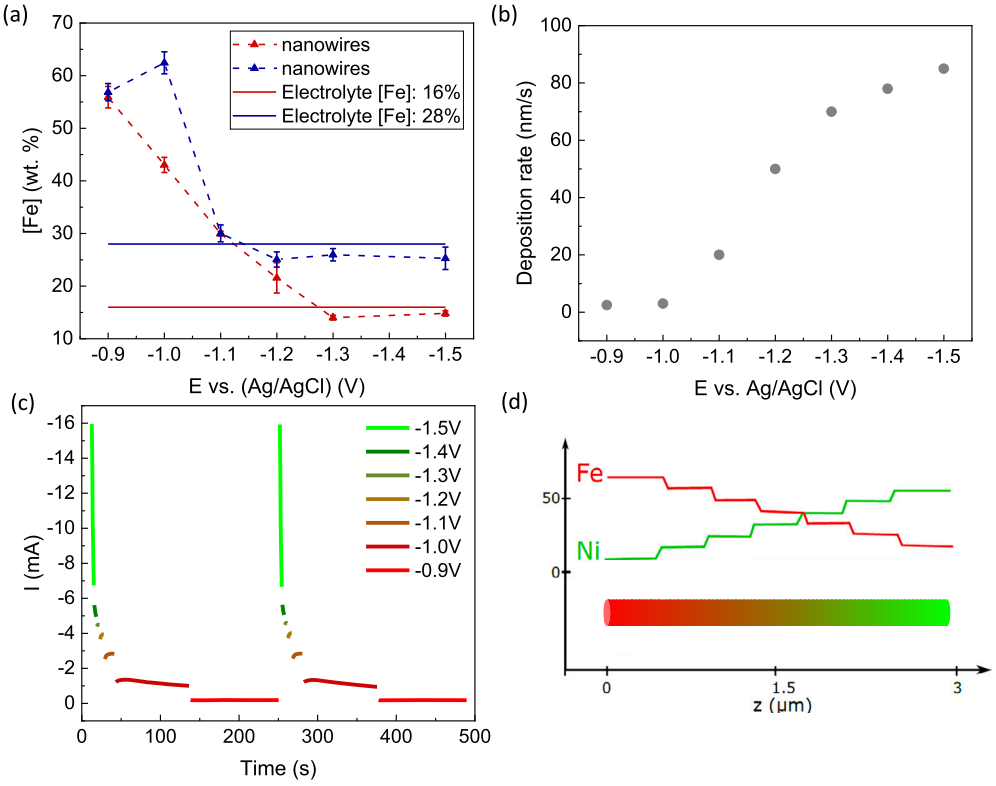

Fig. 2. (a) Composition as a function of the growth potential for two different electrolytes. (b) Deposition rates for the different Fe-Ni composition. (c) Potential pulses used for the growth of the NWs with compositional gradient. (d) Schematics of a segment with a compositional gradient in a cylindrical nanowire. Color-code represents the voltage pulses showed in (c). The vertical axis corresponds to the approximate atomic percentage of Fe (red) and Ni (green). (For interpretation of the colors in the figure(s), the reader is referred to the web version of this article.)

A 30 μm-length permalloy sample ($Ni_{80}Fe_{20}$) was also grown to serve as reference.

Fig. 3.a shows a XAS image measured by TXM at the Fe L_2 X-ray absorption edge in a nanowire grown under the conditions described in Fig. 2.c. In this image, dark areas (low transmission) correspond to Fe-rich regions while brighter areas correspond to Ni-rich regions. As can be seen in the figure, the contrast along the wire changes gradually along the axis in a segment and presents a large jump when a new segment starts. This change in contrast, which is proportional to the amount of Fe in the wire, is clearly observed by plotting the line profile along the length of the NW (Fig. 3.b). The composition was quantified by STEM in Fig. 3.d. The image represents a compositional EDX map at the Fe edge (red) and Ni edge (green) of the STEM image shown in Fig. 3.c. Initially, a majority red color represents a Fe-rich segment. This is followed by an equal mixture of red and green colors, corresponding to a similar atomic percentage of Ni and Fe. As we move towards the right side, the green color increases, and therefore the content in Ni. Finally, the last segment at the right takes again majority of red color, implying the start of a new ratchet segment. The compositional gradient along the axis is visualized in a line profile along the image in (c).

In order to understand the magnetic interactions which occur during the magnetization processes, we have measured the First Order Reversal Curves (FORC) in arrays of NWs. For these measurements, NWs were kept inside the pores of the membrane, and thus magnetic interactions among them play an important role in the magnetic response [30]. In addition, experimental FORC distributions include border effects and other features that might be associated with local inhomogeneity, e.g. different lengths of the NWs. The FORC measurements consisted of the measurement of multiple sequential minor hysteresis loops, beginning at different reversal fields (H_R), and then evolving back to the positive saturation state (see Figs. 4.a and 4.b). Therefore, this technique provides information on the magnetization states of the system not accessible by hysteresis loops. FORC provides statistically averaged results of the whole sample, as in the measurements of hysteresis loops. This aspect contrasts with local probe analysis techniques e.g. Magnetic Force Microscopy, where a limited localized area is characterized. For these local measurements topology and dimensions of the analyzed features can be precisely accounted for. FORC results offer precise information about the magnetic interactions in the sample, including contributions from areas where the response may differ from the average, such as external boundaries. Since the magnetic (dipolar) interactions among NWs play an important role in the magnetic response of NW ensembles, the distance and orientation between NWs must be controlled, so that the signature of intra-wire phenomena signals can be identified and isolated. Thus we performed the experiment on NW assemblies kept inside the membrane pores, where the distance and orientation are statistically controlled. We will not discuss well-known effects such as NWs at the side boundaries of the sample but focus on the most relevant found features. The FORC distribution ρ is calculated through a second-order mixed derivative of magnetization, M, for the externally applied field (H) and the reversal field (H_R) based on the Preisach model [31,32]:

$$\rho(H, H_R) = -\frac{1}{2}\frac{\partial^2 M(H_R, H)}{\partial H \partial H_R} \tag{1}$$

In the FORC diagram (Fig. 4.c) the values of H_U and H_C are defined by:

$$H_C = \frac{H - H_R}{2} \tag{2}$$

$$H_U = \frac{H + H_R}{2} \tag{3}$$

Room temperature hysteresis loops, first magnetization curves and FORC diagrams were measured in a vibrating sample magnetometer (VSM, model Microsense EZ-7). Before the measurements, samples were

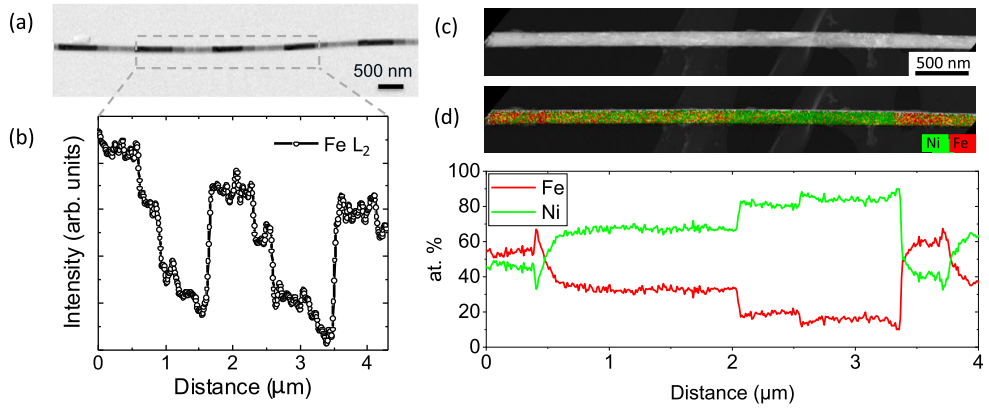

Fig. 3. (a) TXM-XAS image at the Fe-L_2 absorption edge of a ratchet-type Fe-Ni cylindrical nanowire. Periodic gradual changes in composition can be observed. (b) Intensity profile along the wire axis. (c) STEM image of a 100 nm diameter ratchet-type cylindrical nanowire. (d) Top: STEM-EDS compositional map of Ni edge (green) and Fe edge (red). Bottom: Atomic percentage quantification along the axial direction.

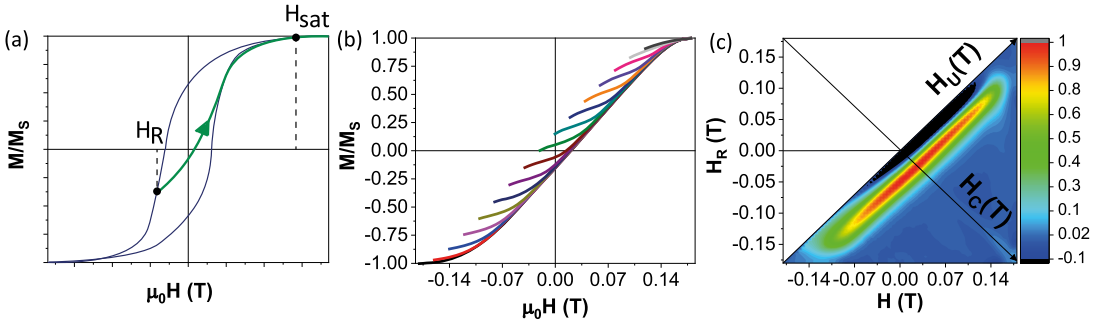

Fig. 4. Scheme of the most representative parameters of FORC distribution. (a) Hysteron (in blue) and first magnetization curve (in green). (b) FORC definition. Measurements start with an applied field of value H_R, with the magnetization measurements along the FORC plotted as function of $M(H_R, H)$ for magnetic field applied from negative to positive values, until reaching the saturation field (H_{sat}). (c) Preisach distribution (or FORC diagram) plotted as a function of H_C and H_U.

submitted to a demagnetization process using an alternating magnetic field along the NWs' main axis, with decreasing amplitude starting from a saturation field of 0.3 T. FORC diagram precision is governed by the magnetic field and reversal field steps, H and H_R, respectively. In this work, the acquisition covered ±0.15 T, performing curves with 5 mT field spacing and a saturating magnetic field of 0.3 T. The time between subsequent measurements was 3 s.

The diagrams summarizing the FORC results are shown in Fig. 5. Panel (a) displays the FORC diagram of an array of permalloy NWs (reference sample). It presents what is usually described as a bent T-shape structure [33–36] with an elongated distribution along the H_U axis, with an interaction field value < 0.075 T, and a less prominent ridge along the H_C axis [37–39], centered at 0.022 T. It is usually assumed that, while strong magnetostatic interactions produce the distribution in the axis of the interaction field, the coercive field distribution can be caused by different factors, some of them intrinsic to the system as chemical composition, while others can be adscribed to length and interwire array distributions.

Samples with gradients in composition (Figs. 5b, 5.c and 5.d) present an evident and substantial deviation from the reference one (Fig. 5.a). The FORC diagrams illustrate the expected elongated distributions along H_U, associated with strong magnetostatic interactions, and located at similar H_C values (0.025-0.014 T) to those observed in (a). However, these distributions are not symmetric along H_U axis but appear distorted. In the cases (c) and (d), in addition, an asymmetric negative interaction field distribution (a negative FORC density ridge) arises at low H_C fields, shifted towards positive H_U values. These asymmetries increase for stronger composition gradients.

Negative values in FORC distributions arise in complex nanosystems [40,41] and magnetic exchange springs [42] where multiple coupled magnetic phases co-exist. The appearance of distorted features is also confirmed due to high-speed variations of the magnetic fields during the measurements [43]. In the present case we have to note that all samples have been measured at the same moderate speed. However, to the best of our knowledge, the observed FORC distributions are not commonly present in NW array systems. The only mention of similar FORC distributions of NW arrays was recently reported and discussed for Ni-Fe-Ga-NW arrays [44] in terms of structural phase change, but certainly not evidenced or hypothesized for other types of NW array systems. In our case, we can exclude the interpretation of this negative ridge solely as a statistical distribution of hysterons or an artifact due to a fast measurement rate. The negative distributions for the (b-d) samples resemble populations of hysterons with similar H_C and asymmetrical distributed H_U. This allows us to rule out pure dipolar magnetostatic type interactions as their main physical origin. Moreover, the positive distributions associated with magnetostatic interactions, similar to that of the reference sample (a), appear distorted. This should be linked to the modulation of the composition of the NWs (magnetic ratchet) and its effect on the collective magnetic response of the array, compared to a regular NW array. The negative distributions for the (b-d) samples resemble populations of hysterons with similar H_C and asymmetrical distributed H_U. This excludes pure dipolar magnetostatic type interactions as their main physical origin.

We propose the hypothesis that these facts are compatible with the complex combined existence of similar energy barriers inside an inhomogeneous magnetic field in the system. The negative distributions, with similar narrow values of H_C i.e. similar energy level for the chemical modulated NW samples endorse the existence of energy barriers inside the NW array. The inhomogeneous magnetic field arises from the finite length of the NWs (30 μm). In this scenario, the magnetic

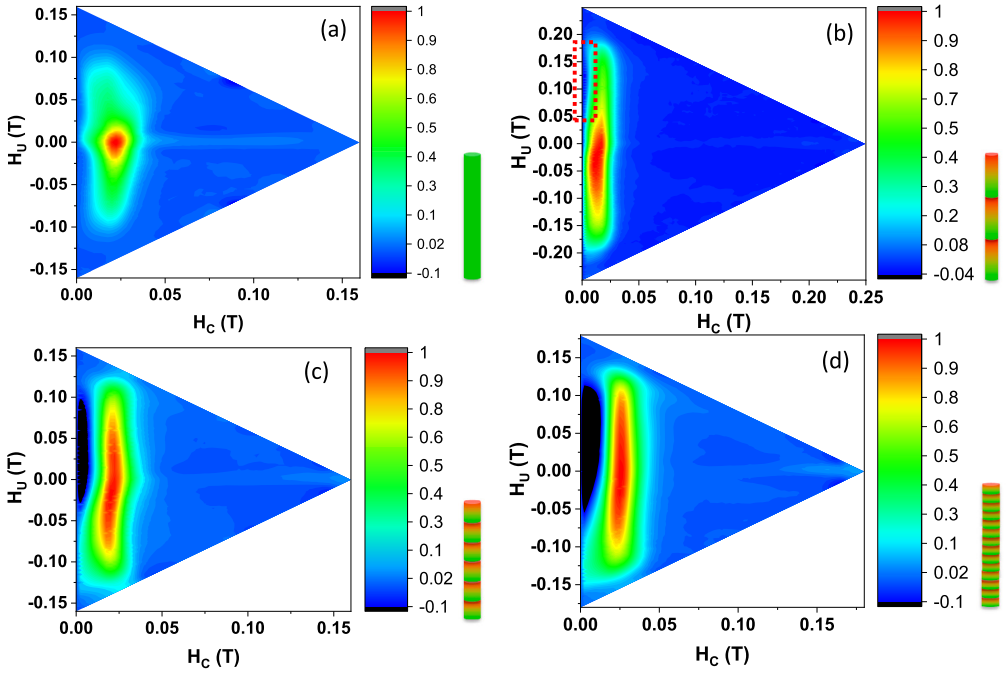

Fig. 5. FORC diagrams measured in NWs' arrays of 30 μm in length. (a) Reference sample, Permalloy NWs. (b-d) NWs with gradients in composition where the content of Fe and Ni changes from $Fe_{20}Ni_{80}$ to $Fe_{70}Ni_{30}$. The length of the chemical gradient in each sample is 4 μm, 2 μm and 1 μm, respectively. On the right side of the scale bar it is shown a schematic of the chemical configuration of the NWs, where green corresponds with $Fe_{10}Ni_{90}$ and red with $Fe_{65}Ni_{35}$.

field at the top/bottom edges is different than that in the center. Therefore, each chemical gradient located at different position, within the NWs of the array, experiences a heterogeneous global magnetic field. This magnetic field is not static. It changes dynamically according to the magnetization state of each NW or each segment of the NW. The magnetization reversal of NWs in this type of arrays is an asynchronous process [45]. The magnetization in single continuous NW initiates with the nucleation of a domain wall at its edge and evolves by its fast propagation along NW. But, in this case due to chemical gradients, these domain walls can nucleate not only at the edges of the NW and also in the edges of each segment containing a chemical gradient. In addition, they will experience pinning effects in their propagation along the NW. However, and as we mentioned above, we cannot expect that all the domain walls of each NW do propagate synchronously in all NW at the same time. Most probably, some domain walls will remain pinned meanwhile some domain walls of surrounding NWs will have enough energy to overtake the energy barriers. These events modify the local field and may induce the reversible backward motion of those domain walls that previously were pinned due to the chemical gradient [41]. Note that the backward motion is limited between the two peaks of Fe concentration. This situation will be equivalent to a soft/hard phase coupling [42]. This justifies the negative FORC distribution with values of H_C close to the positive one. Moreover, it is evidenced by the asymmetric and the distorted positive distribution associated with magnetostatic interactions. The observed broadening of H_C with the shorter length of chemical gradients, is a direct consequence of the existence of larger number of energy barriers and their statistical value spreading.

To sum up, we have demonstrated the experimental realization of introducing gradual changes in composition in Fe-Ni ferromagnetic NWs along their axis via electrodeposition process. The distortions observed in the FORC diagrams of the NWs with chemical gradients compared to the one of the reference sample, (distortions that are larger for larger gradients), are the first indirect evidence of asymmetry in the magnetization process induced during the growth in cylindrical NWs. Although more direct evidence on domain wall motion may be extracted in the future from micromagnetic simulations or measurements on individual nanowires, the results shown in this work clearly indicate that a variation in composition along the axis allows tuning the energy landscape for the domain wall motion, which is reflected in asymmetric magnetization processes, paving the way toward full control of the movement of domain walls along these NWs.

Declaration of competing interest

The authors declare that they have no known competing financial interests or personal relationships that could have appeared to influence the work reported in this paper.

Acknowledgements

We thank Prof. D. Gilbert for his suggestions and comments. This work has been partially funded by MCIN/AEI/10.13039/501100011033 through Projects PID2020-117024GB-C43, PID2020-115325GB-C31 and TED2021-130957B-C52 and by the Comunidad de Madrid through Project No. NANOMAGCOST-CM P2018/NMT-4321. IMDEA Nanociencia acknowledges support from the Severo Ochoa Programme for Centres of Excellence in R&D (Grants No. SEV-2016-0686 and No. CEX2020-001039-S). The ALBA in-house research program has supported the work. We thank the Spanish National Center of Electron Microscopy for Scanning Electron Microscopy measurements. Sandra Ruiz-Gómez acknowledges the support of the Alexander von Humboldt Foundation and the European Union under the Marie Skłodowska-Curie grant agreement 101061612.

References

[1] D.A. Allwood, G. Xiong, C.C. Faulkner, D. Atkinson, D. Petit, R.P. Cowburn, Magnetic domain-wall logic, Science 309 (2005) 1688–1692.
[2] Z. Luo, A. Hrabec, T.P. Dao, G. Sala, S. Finicio, J. Feng, S. Mayr, J. Raabe, P. Gambardella, L. Heyderman, Current-driven magnetic domain logic, Nature 579 (2020) 214.
[3] S.S.P. Parkin, M. Hayashi, L. Thomas, Magnetic domain-wall racetrack memory, Science 320 (2008) 190–194.
[4] S.S.P. Parkin, S.-H. Yank, Memory on the racetrack, Nat. Nanotechnol. 10 (2015) 195–198.
[5] J. Akerman, M.M. noz, M. Maicas, J.L. Prieto, Stochastic nature of the domain wall depinning in permalloy magnetic nanowires, Phys. Rev. B 82 (2010) 064426.

[6] R. Lavrijsen, J.-H. Lee, A. Fernández-Pacheco, D.C.M.C. Petit, R. Mansell, R.P. Cowburn, Magnetic ratchet for three-dimensional spintronic memory and logic, Nature 493 (2013) 647–650.
[7] C. Castán-Guerrero, J. Herrero-Albillos, J. Sesé, J. Bartolomé, F. Bartolomé, A. Hierro-Rodriguez, F. Valdés-Bango, J. Martín, J. Alameda, L. Garcia, Submicrometric 2D ratchet effect in magnetic domain wall motion, Physica B, Condens. Matter 455 (2014) 76–78.
[8] J. Cui, S.M. Keller, C.Y. Liang, G.P. Carman, C.S. Lynch, Nanoscale magnetic ratchets based on shape anisotropy, Nanotechnology 28 (2017) 08LT01.
[9] J.H. Franken, H.J.M. Swagten, B. Koopmans, Shift registers based on magnetic domain wall ratchets with perpendicular anisotropy, Nat. Nanotechnol. 7 (2012) 499–503.
[10] A. Fernandez-Pacheco, R. Streubel, O. Fruchart, R. Hertel, P. Fischer, R.P. Cowburn, Three-dimensional nanomagnetism, Nat. Commun. 8 (2017) 15756.
[11] R. Streubel, P. Fischer, F. Kronast, V.P. Kravchuk, D.D. Sheka, Y. Gaididei, O.G. Schmidt, D. Makarov, Magnetism in curved geometries, J. Phys. D, Appl. Phys. 49 (2016) 363001.
[12] A. Wartelle, B. Trapp, M. Staňo, C. Thirion, S. Bochmann, J. Bachmann, M. Foerster, L. Aballe, T.O. Menteş, A. Locatelli, A. Sala, L. Cagnon, J.-C. Toussaint, O. Fruchart, Bloch-point-mediated topological transformations of magnetic domain walls in cylindrical nanowires, Phys. Rev. B 99 (2019) 024433.
[13] M. Schöbitz, A.D. Riz, S. Martin, S. Bochmann, C. Thirion, J. Vogel, M. Foerster, L. Aballe, T. Mentes, A. Locatelli, F. Genuzio, S. Le-Denmat, L. Cagnon, J.C. Toussaint, D. Gusakova, J. Bachmann, O. Fruchart, Fast domain wall motion governed by topology and oersted fields in cylindrical magnetic nanowires, Phys. Rev. Lett. 123 (2019) 217201.
[14] D. Sanz-Hernández, C. Donnelly, L. Pérez, A. Fernández-Pacheco, Nanofabrication of three-dimensional magnetic structure, in: J.M. de Teresa (Ed.), Nanofabrication: Nanolithography Techniques and Their Applications, IOP Publishing, Bristol, 2020.
[15] S. Ruiz-Gómez, C. Fernández-González, L. Perez, Electrodeposition as a tool for nanostructuring magnetic materials, Micromachines 13 (2022) 1223.
[16] A. Nunez, L. Pérez, M. Abuín, J.P. Araujo, M.P. Proenca, Magnetic behaviour of multisegmented FeCoCu/Cu electrodeposited nanowires, J. Phys. D, Appl. Phys. 50 (2017) 155003.
[17] L. Sun, Y. Hao, C.-L. Chien, P.C. Searson, Tuning the properties of magnetic nanowires, IBM J. Res. Dev. 49 (2005) 79–102.
[18] M. Chen, C.-L. Chien, P.C. Searson, Potential modulated multilayer deposition of multisegment Cu/Ni nanowires with tunable magnetic properties, Chem. Mater. 18 (6) (2006) 1595–1601.
[19] C. Bran, J.A. Fernandez-Roldan, R.P. del Real, A. Asenjo, O. Chubykalo-Fesenko, M. Vazquez, Magnetic configuration in modulated cylindrical nanowires, Nanomaterials 11 (2021) 600.
[20] E. Berganza, C. Bran, M. Jaafar, M. Vázquez, A. Asenjo, Domain wall pinning in FeCoCu bamboo-like nanowires, Sci. Rep. 6 (2016) 29702.
[21] L.A. Rodríguez, C. Bran, D. Reyes, E. Berganza, M. Vázquez, C. Gatel, E. Snoeck, A. Asenjo, Quantitative nanoscale magnetic study of isolated diameter-modulated FeCoCu nanowires, ACS Nano 10 (10) (2016) 9669–9678.
[22] S. Ruiz-Gómez, C. Fernández-González, E. Martínez, V. Raposo, A. Sorrentino, M. Foerster, L. Aballe, A. Mascaraque, S. Ferrer, L. Pérez, Helical surface magnetization in nanowires: the role of chirality, Nanoscale 12 (2020) 17880–17885.
[23] S. Ruiz-Gomez, M. Foerster, L. Aballe, M.P. Proenca, I. Lucas, J.L. Prieto, A. Mascaraque, J. de la Figuera, A. Quesada, L. Pérez, Observation of a topologically protected state in a magnetic domain wall stabilized by a ferromagnetic chemical barrier, Sci. Rep. 8 (2018) 16695.
[24] L. Álvaro-Gómez, S. Ruiz-Gómez, C. Fernández-González, M. Schöbitz, N. Mille, J. Hurst, D. Tiwari, A. De Riz, I.M. Andersen, J. Bachmann, L. Cagnon, M. Foerster, L. Aballe, R. Belkhou, J.-C. Toussaint, C. Thirion, A. Masseboeuf, D. Gusakova, L. Pérez, O. Fruchart, Micromagnetics of magnetic chemical modulations in soft-magnetic cylindrical nanowires, Phys. Rev. B 106 (2022) 054433.
[25] A. Himeno, K. Kondo, H. Tanigawa, S. Kasai, T. Ono, Domain wall ratchet effect in a magnetic wire with asymmetric notches, J. Appl. Phys. 103 (2008) 07E703.
[26] C. Bran, E. Berganza, J.A. Fernandez-Roldan, E.M. Palmero, J. Meier, E. Calle, M. Jaafar, M. Foerster, L. Aballe, A.F. Rodriguez, R.P. del Real, A. Asenjo, O. Chubykalo-Fesenko, M. Vazquez, Magnetization ratchet in cylindrical nanowires, ACS Nano 12 (2018) 5932–5939.
[27] A. Sorrentino, J. Nicolas, R. Valcarcel, F.J. Chichon, M. Rosanes, J. Avila, A. Tkachuk, J. Irwin, S. Ferrer, E. Pereiro, MISTRAL: a transmission soft X-ray microscopy beamline for cryo nano-tomography of biological samples and magnetic domains imaging, J. Synchrotron Radiat. 22 (2015) 1112.
[28] A. Llavona, L. Pérez, M.C. Sánchez, V.D. Manuel, Enhancement of anomalous codeposition in the synthesis of Fe-Ni alloys in nanopores, Electrochim. Acta 106 (2013) 392–397.
[29] A. Brenner, Electrodeposition of Alloys: Principles and Practice, vol. 1, Academic Press Inc., 1963.
[30] M. Vazquez, Cylindrical nanowire arrays: from advanced fabrication to static and microwave magnetic properties, J. Magn. Magn. Mater. 543 (2022) 168634.
[31] I. Mayergoyz, Mathematical models of hysteresis, IEEE Trans. Magn. 22 (5) (1986) 603–608.
[32] C.R. Pike, A.P. Roberts, K.L. Verosub, Characterizing interactions in fine magnetic particle systems using first order reversal curves, J. Appl. Phys. 85 (9) (1999) 6660–6667.
[33] T. Peixoto, D. Cornejo, Characterizing magnetic interactions in Ni nanowires by FORC analysis, J. Magn. Magn. Mater. 320 (14) (2008) e279–e282.
[34] P. Sergelius, J.G. Fernandez, S. Martens, M. Zocher, T. Böhnert, V.V. Martinez, V.M. De La Prida, D. Görlitz, K. Nielsch, Statistical magnetometry on isolated NiCo nanowires and nanowire arrays: a comparative study, J. Phys. D, Appl. Phys. 49 (14) (2016) 145005.
[35] E.M. Palmero, F. Béron, C. Bran, R.P. Del Real, M. Vázquez, Magnetic interactions in compositionally modulated nanowire arrays, Nanotechnology 27 (43) (2016) 435705.
[36] X. Kou, X. Fan, R.K. Dumas, Q. Lu, Y. Zhang, H. Zhu, X. Zhang, K. Liu, J.Q. Xiao, Memory effect in magnetic nanowire arrays, Adv. Mater. 23 (11) (2011) 1393–1397.
[37] M.P. Proenca, C.T. Sousa, J. Ventura, J. Garcia, M. Vazquez, J.P. Araujo, Identifying weakly-interacting single domain states in Ni nanowire arrays by FORC, J. Alloys Compd. 699 (2017) 421–429.
[38] C.-I. Dobrotă, A. Stancu, What does a first-order reversal curve diagram really mean? A study case: array of ferromagnetic nanowires, J. Appl. Phys. 113 (4) (2013) 043928.
[39] A. Pierrot, F. Béron, T. Blon, FORC signatures and switching-field distributions of dipolar coupled nanowire-based hysterons, J. Appl. Phys. 128 (9) (2020) 093903.
[40] F. Béron, A. Kaidatzis, M.F. Velo, L.C. Arzuza, E.M. Palmero, R.P. Del Real, D. Niarchos, K.R. Pirota, J.M. García-Martín, Nanometer scale hard/soft bilayer magnetic antidots, Nanoscale Res. Lett. 11 (1) (2016) 1–11.
[41] A. Ruiz-Clavijo, O. Caballero-Calero, D. Navas, A.A. Ordonez-Cencerrado, J. Blanco-Portals, F. Peiró, R. Sanz, M. Martín-González, Unveiling the complex magnetization reversal process in 3D nickel nanowire networks, Adv. Electron. Mater. 8 (2022).
[42] D.A. Gilbert, P.D. Murray, J.D. Rojas, R.K. Dumas, J.E. Davis, K. Liu, Reconstructing phase-resolved hysteresis loops from first-order reversal curves, Sci. Rep. 11 (2021) 4018.
[43] P. Andrei, O. Caltun, A. Stancu, Rate dependence of first-order reversal curves by using a dynamic Preisach model of hysteresis, Physica B 372 (2006) 265–268.
[44] M. Varga, L. Galdun, B. Kunca, V. Vega, J. GarcÃa, V.M. Prida, E. Barriga-Castro, C. Luna, P. Diko, K. Saksl, R. Varga, FORC and TFORC analysis of electrodeposited magnetic shape memory nanowires array, J. Alloys Compd. 897 (2022) 163211.
[45] Y.P. Ivanov, M. Vázquez, O. Chubykalo-Fesenko, Magnetic reversal modes in cylindrical nanowires, J. Phys. D, Appl. Phys. 46 (2013) 485001.